scientific reports

Check for updates

OPEN

Innovative biopolymers composite based thin film for wound healing applications

Majid Ali[1,2]✉, Shakir Ullah[1], Shaker Ullah[1], Muhammad Shakeel[1,2], Tayyaba Afsar[3], Fohad Mabood Husain[3,4], Houda Amor[5] & Suhail Razak[3]✉

Efficient wound and burn healing is crucial for minimising complications, preventing infections, and enhancing overall well-being, necessitating the development of innovative strategies. This study aimed to formulate a novel thin film combining chitosan, carboxymethyl cellulose, tannic acid, and beeswax for improved wound healing applications. Several formulations, incorporating chitosan, carboxymethyl cellulose, tannic acid, and beeswax in various percentages, were utilized to deposit thin films via the solvent evaporation technique, Mechanical properties, morphology, antioxidant activity, antibacterial efficacy, and wound healing potential were evaluated. The optimized thin film (M4), composed of 2% chitosan, 2% carboxymethyl cellulose, and 1% tannic acid, along with 0.2% glycerol and 0.2% tween80, exhibited a thickness of 39.0 ± 1.14 µm and a tensile strength of 0.275 ± 0.003 MPa. It demonstrated a swelling degree of 283.0 ± 2.0% and a drug release capacity of 89.4% within 24 h. The film also showed a low contact angle of 40.5° and a water vapour transmission rate of 1912.25 ± 13.10 g m^{-2} 0.24 h^{-1}. FT-IR spectroscopy indicated that chitosan and carboxymethyl cellulose were cross-linked through amide linkages, with tannic acid occupying the interstitial spaces and hydrogen bonding stabilizing the structure. Microscopy of M4 revealed a uniform morphology. The film exhibited strong antioxidant activity of (95.17 ± 0.02%) and antibacterial efficiency (80.8%) against *S. aureus*. In a rabbit model, the film significantly enhanced burn and excision wound recovery, with 90.0 ± 3.3% healing for burns and 88.85 ± 1.7% for infected wounds by day 7. Complete skin regeneration was observed within 10–12 days. The M4 thin film demonstrated exceptional mechanical properties and bioactivity, offering protection against pathogens and promoting efficient wound healing. These findings suggest its potential for further investigation in treating various infections and its role in developing novel therapeutic interventions.

Keywords Thin film, Wound healing, Burn, Infection, Antioxidant, Antibacterial, Chitosan, Carboxymethyl cellulose, Tannic acid

Abbreviations

BW	Beeswax
CMC	Carboxymethyl cellulose
CS	Chitosan
dH_2O	Distilled water
MCA	Monochloroacetic acid
S	Supplementary
TA	Tannic acid
WVTR	Water vapor transmission rate

The skin, the body's largest organ, is crucial in protecting against foreign invaders and maintaining homeostasis. In the event of damage, such as cuts or burns, it is important to cover the affected area with a protective coating to prevent infection by microorganisms[1]. An ideal wound dressing should possess appropriate mechanical

[1]Department of Chemistry, Government Postgraduate College No. 1, Abbottabad 22010, KPK, Pakistan. [2]Department of Higher Education Archives and Library, Government of Khyber Pakhtunkhwa, Peshawar, Pakistan. [3]Department of Community Health Sciences, College of Applied Medical Sciences, King Saud University, Riyadh, Saudi Arabia. [4]Department of Food Science and Nutrition, College of Food and Agriculture Sciences, King Saud University, Riyadh 11451, Saudi Arabia. [5]Department of Obstetrics, Gynecology and Reproductive Medicine, Saarland University Clinic, Homburg, Germany. ✉email: hm.ali6584@gmail.com; smarazi@ksu.edu.sa

properties, absorb exudates from the wound while maintaining a proper moist environment, facilitate gaseous exchange, guard against infection and pathogens, exhibit biocompatibility and biodegradability, reduce pain, and be cost-effective[2]. Efficient wound and burn healing is vital for minimising complications, preventing infections, and enhancing overall well-being[3].

Thin films made of polymers have several advantages, including the absorption of exudates from the wound surface and providing a high water vapour transmission rate[4]. Additionally, they offer protection against microbial growth[3,5]. Extensive studies have been conducted on biopolymers to improve wound healing, tissue engineering and artificial skin[3,6]. The scientific community frequently reports starch and cellulose derivatives, chitosan, alginates, beeswax, carnauba wax, free fatty acids, proteins such as casein, whey, and gluten, polyhydroxybutyrates, polylactic acid, polycaprolactone, polyvinyl alcohol, polybutylene succinate, and polyglycolic acid as the most prevalent types of biopolymers[4,7].

Chitosan (CS), one of these polymers, possesses biocompatibility, biodegradability, and bioactivity, making it suitable for use in various biomedical applications[4]. It also can form complexes with anionic biomaterials[8]. However, strengthening its mechanical, chemical, and biological properties is crucial to maximizing its utility[9]. Various scientists chemically modified chitosan to improve its properties and functionality[10]. Cellulose is anticipated to serve as a supportive material for chitosan, ensuring adequate mechanical strength, and both exhibit good compatibility owing to their structural similarity[11]. Carboxymethyl cellulose (CMC) is an anionic partially water-soluble derivative of cellulose, where its solubility greatly depends on degree of substitution[12]. It is used for various drug delivery and tissue engineering applications[13]. The carboxyl group allows for chemical crosslinking (a covalent interaction) between CMC and the amino group of chitosan, using various crosslinking agents such as glutaraldehyde, genipin, and epichlorohydrin[14]. Another possibility is physical crosslinking, which may occur through electrostatic interactions between two oppositely charged groups or physical entanglement through hydrogen bonding[12]. According to Guarnizo-Herrero et al.. the primary interactions in the creation of polyelectrolyte, involve the electrostatic attractions between the ionized amino (NH_3^+) group of chitosan and the carboxylic (COO^-) groups of the anionic polymer[11]. Uyanga and Daoud recently investigated the effect of crosslinkers such as fumaric acid, tartaric acid, citric acid and zinc ions on CMC-CS composite hydrogel[14]. Valizadeh et al.. synthesized a bioactive composite film from chitosan and carboxymethyl cellulose using glutaraldehyde, cinnamon essential oil and oleic acid as crosslinkers[16].

Tannic acid (TA) is a gallic ester of D-glucose in which the hydroxyl groups of the carbohydrate are esterified with gallic acid dimers. Its polyphenolic groups can interact with biological macromolecules[17,18]. Tannic acid (TA) exhibits potent astringent, antioxidant, hemostatic, and antibacterial properties, making it valuable not only in industry but also in the medical field. It has proven to be effective as a treatment for skin ulcers, burns, wounds, and toothache[18]. It has antimutagenic, antitumor, and antioxidant activity[19]. The antimicrobial and wound-healing properties of tannic acid have been demonstrated in various studies; however, the administration of an uncontrolled dosage may lead to undesirable side effects[18]. Notably, when tannic acid polyphenols are cross-linked with polymeric materials, forming a robust composite incorporates the advantageous properties of this tannin[19,20].

Various natural polymers and their combinations have been examined for wound dressing and healing applications[4,21]. For instance, Adeli et al.. investigated the wound-healing activity of nanofibrous mats composed of polyvinyl alcohol, chitosan, and starch[1]. Kaczmarek et al.. reported on thin films made from a mixture of chitosan and tannic acid for wound dressing[19]. Xu et al.. explored composite nanofibers made of chitosan, tannic acid, and pullulan for wound dressing applications[18]. Liang et al.. studied the effects of adding royal gel to a chitosan matrix for wound dressing[8]. Khorasani et al.. incorporated ZnO nanoparticles into polyvinyl alcohol/chitosan hydrogels to investigate wound healing applications[3]. Asanarong et al.. explored bacterial cellulose loaded with papain composites for wound dressing[11]. Guarnizo-Herrero et al.. reported sustained release of clarithromycin from a matrix of chitosan and sodium carboxymethyl cellulose[12]. Uyanga and Daoud recently investigated effect of crosslinkers such as fumaric acid, tartaric acid, citric acid and zinc ions on carboxymethyl cellulose-chitosan composite hydrogel[22]. Recently, Parin et al. investigated novel PVA/CMC/HPO Pickering sponges for wound healing applications[23]. Abdallah et al.. developed chitosan biquanidine (ChBG) nanoparticles through a one-pot green synthesis as a highly effective anti-tuberculosis drug[24]. Abu Elella et al.. designed antibacterial hydrogels using cationic trimethyl chitosan chloride and carboxymethyl starch.

However, despite these advancements, the synthesis of a thin film combining chitosan, carboxymethyl cellulose, and tannic acid is a novel approach, which distinguishes this study from previous work. The unique combination of these materials has not been explored before for wound healing applications, and this is the primary focus of this research. This work represents a significant departure from previous studies by developing a new material with enhanced properties for wound healing, such as improved biocompatibility, mechanical strength, and antimicrobial activity.

Materials and methods

Collection of materials

All chemicals and solvents used in this study were of analytical grade and sourced from Merck. To create the thin film, medium molecular weight chitosan (161.156) (CAS No. 9012-76-4, Product No. 448877) with an 85% degree of deacetylation was utilized. Tannic acid was acquired from BDH Chemical Ltd (Product No. 30337). Cellulose (CAS No. 9004-34-6, Product No. 11363) was converted into carboxymethyl cellulose (CMC). Other chemicals, including refined beeswax (CAS No. 8012-89-3), monochloroacetic acid (Product No. 800412), sodium hydroxide (CAS No. 1310-73-2), glycerol 87% (Product No. 28454), Tween80 (Product No. 46987), acetic acid (CAS No. 64-19-7), methanol (K2133256-820), and ethanol (CAS No. 64-17-5) were also used. All solutions were prepared using distilled water (dH_2O). All methods followed relevant guidelines and regulations, and the study is reported in accordance with ARRIVE guidelines.

Preparation of carboxymethyl cellulose

Cellulose was converted into carboxymethyl cellulose as described by Rachtanapun et al.[15]. Cellulose powder (7.5 g) was mixed with 15 mL of a 30% NaOH solution and 225 mL of isopropanol on a magnetic stirrer for 30 min. For carboxymethylation, 9 g of monochloroacetic acid (MCA) was added to the solution. The mixture underwent continuous stirring at 55 °C for 30 min, covered with aluminium foil and placed in an oven at 65 °C for 3.5 h. Following the heating process, the solution underwent phase separation, resulting in two distinct phases. The liquid phase was discarded, and the solid phase was re-suspended in methanol. For each 80 mL of suspension, 100 mL of acetic acid was used for neutralization, followed by filtration. The final product was washed three times with 70% ethanol and then washed with methanol. The Carboxymethyl Cellulose (CMC) was dried at 55 °C for 2 h and stored at room temperature for further use.

Formulation and deposition of thin films

Multiple formulations (M1-5) were developed for the synthesis of thin films by blending chitosan (CS), carboxymethyl cellulose (CMC), tannic acid (TA), and beeswax (BW) in varying proportions, based on established methodologies from previous studies, with slight modifications[16,18,19,22]. In M1, 1% CS was dissolved in 50 mL of 1% acetic acid solution, in which 1% CMC and 0.5% TA were dissolved with constant stirring and heating up to 70 °C. In M2, 1% CS, 1% CMC and 0.5% TA were dissolved similarly, and 0.2% glycerol and 0.2% tween80 were added for emulsification. In M3, 2% CS was dissolved in 50 mL of 1% acetic acid, and 2% CMC and 1% TA was dissolved in the same solution. In M4, 2% CS, 2% CMC, and 1% TA was dissolved similarly, and 0.2% glycerol and 0.2% tween80 were added. In M5, 1% CS, 1% CMC, 0.5% TA and 1% BW were added similarly, along with emulsifying agents 0.2% glycerol and 0.2% tween80 at constant stirring and heating up to 70 °C[25–27]. The hot solution was poured into a glass plate with a diameter of 9 cm, and a thin film was obtained after the evaporation of the solvent in an oven at 30 °C for 36 h. All the combinations of thin films from M1 to M5 are presented in a Table 1.

Characterization of thin films

Thickness and tensile strength

The thickness of the films (M2–5) was determined using a handheld micrometer. For each thin film, measurements were taken at random locations (a total of 5), and the average thickness was calculated. The thickness of each film was re-measured after swelling in water for 2 h. The tensile strength of the films was assessed using a bursting strength tester (Model: PBG-400).

Swelling degree

The swelling degree of films was determined following the methodology described by Saragih et al.[28]. Dried thin film pieces were cut into 1 cm^2 and weighed initially to obtain the dried mass (W_d). Subsequently, these films were immersed in dH_2O at 37 °C by using a water bath (Model: HH-S4), and the wet weight of the films (W_w) was recorded after 2 h. The swelling degree was calculated using the formula:

$$\text{Swelling degree } (\%) = [(W_w - W_d) / W_d] \times 100$$

Contact angle

The wettability of thin films was assessed by measuring the contact angles, following the procedure described by Bandyopadhyay et al.[7]. A droplet of 10 µL of dH_2O was carefully dispensed onto the horizontal surface of the hydrogel thin film using a micropipette. High-resolution images were captured using a built in micro camera of Samsung Note 9. The contact angle was then measured with the assistance of the "Angle Meter" mobile application.

Degree of crosslinking

The assessment of crosslinking in thin films M3 and M4 followed the methodology outlined by Saragih et al.[28] The weight of the films was measured before (W_g) and after immersing them in chloroform for 24 h (W_o). The calculation of the degree of crosslinking involved applying the following equation:

$$\text{Degree of Crosslinking } (\%) = (W_g/W_o) \times 100$$

Films	CS	CMC	TA	BW	Glycerol	Tween80
M1	1%	1%	0.5%	–	–	–
M2	1%	1%	0.5%	–	0.2%	0.2%
M5	1%	1%	0.5%	1%	0.2%	0.2%
M3	2%	2%	1%	–	–	–
M4	2%	2%	1%	–	0.2%	0.2%

Table 1. Composition of Thin films (M1 to M5) including chitosan, carboxymethyl cellulose, tannic acid, beeswax, glycerol, and tween 80.

Water vapor transmission rate

To assess the water vapor transmission rate (WVTR), following the methodology reported by Adeli et al.. circular pieces of the films (M3, M4, and M5) were cut and affixed to the mouths of conical flasks with a diameter of 0.018 m and exposure area (A) of 0.0002545 m^{-2}, each containing 25 mL of water[1]. Subsequently, the bottles were weighed (W_i), and then incubated at a temperature of 35 °C in a water bath (Model: HH-S4). After 24 h, the bottles were removed from the water bath, and their weights were measured again (W_f). The WVTR of the thin film was calculated using the following formula:

$$\mathrm{WVTR} = (W_i - W_f) / A \left(g\,m^{-2}\,day^{-1}\right)$$

Drug release capacity

The release of tannic acid from the films, M3 and M4, each weighing 100 mg and containing approximately 20 mg of tannic acid, was assessed by immersing them in 20 mL of distilled water at room temperature. The concentration of tannic acid in dH_2O was determined by measuring absorption at 276 nm using a UV/Vis spectrophotometer (SP-UV1100). Readings were initially recorded at 15-minute intervals and subsequently at 1-h and 2-h intervals, up to 24 h. The concentration (in ppm, i.e., 0.1 mg/mL) was calculated by plotting a standard curve of tannic acid up to a concentration of 100 ppm, and the data were interpolated using OriginPro 6.1 software. A dilution factor of five to ten times was applied based on the sample concentration in the solution. The percentage of drug release was calculated relative to the initial concentration of tannic acid present in the thin film immersed in water. The plot depicting the percentage of drug release over time was created using GraphPad Prism 9 software.

The drug release kinetics of the M4 thin film was analyzed using the Higuchi model, which is based on diffusion-controlled release mechanisms[29,30]. This model describes an initial rapid release of the drug followed by a slower, sustained release driven by diffusion through the polymer matrix. The cumulative percentage of drug release was plotted against the square root of time to evaluate the fit of the data to the Higuchi model. Linear regression analysis was conducted using GraphPad Prism 9 software, and the goodness of fit (R^2) and statistical significance (p-value) were determined[29].

FT-IR analysis

FT-IR spectroscopy was employed to ascertain the functional groups and crosslinking of polymers in the thin film. The IR spectra of the CS, CMC, TA, and M4 thin films were captured using a spectrophotometer (Model: 233 Nicolet 6700 spectrophotometer, USA), and the analysis was performed by comparing the spectra obtained through OriginPro 6.1 software.

Microstructure of thin films

The microstructures of thin films (M3, M4, M5) were examined using the electric binocular compound microscope (Model: 500) at a 5× magnification. Images were captured with a microscopic USB digital camera (ALT-350).

Antioxidant activity

The antioxidant capability of the M3 and M4 thin films was assessed through DPPH free radical scavenging activity as described by Basker et al.[31]. Each 2×2 cm thin film sample was immersed in 2 mL of DPPH solution in methanol and left to incubate in darkness at room temperature. Color changes were monitored at 517 nm using a UV/Visible spectrophotometer (SP-UV1100) at 30-minute intervals over a 2-h period[32]. Samples were taken in triplicate, and the control consisted of a DPPH solution with 0.1 mL of dH_2O. The percentage inhibition was calculated using a formula:

$$\%\ \mathrm{Inhibition} = [(A_o - A_1)\ /A_o] \times 100$$

Antibacterial activity

The antibacterial efficacy of the M4 thin films was assessed using the disc diffusion method against both Gram-positive (*S. aureus*) and Gram-negative (*E. coli*) bacteria, both implicated in skin and wound infections[33]. In this method, as described by Liang et al.. and Parin et al. a bacterial suspension of 100 µL was cultured on sterilized nutrient agar plates at 37 °C for 24 h. Circular hydrogel M4 films, with a diameter of 6 mm, were then placed in contact with the agar plates. Following a 24-h incubation period at 37 °C, photographs were taken of the inhibition zones, which are halos around the specimens indicating no bacterial growth. Amoxicillin (10 µg/disc) served as the positive control, while DMSO functioned as the negative control[8,33].

Wound healing activity

For wound healing activity, healthy male rabbits aged 4–5 months, weighing about 1.6–2 kg were purchased from the local market and kept under observation for several days before the start of the experiment. Approval for the research was obtained from the Institutional Animal Care and Use Committee (IACUC) with D. No. 116. Wound closure duration, and the healing process were examined using excision, burn, and infected wound models. Local anesthesia with 0.5 ml of Lidoject 2% was administered to the rabbits, and their dorsal pelvic region was shaved. Wounds were induced using a surgical blade, removing skin in an area of approximately 1 cm × 1 cm with a depth of 2–3 mm. Burns were produced by a 1.5 cm × 1.5 cm hot metal plate. Rabbit models A1 and A2 were used for excision wounds, B1 and B2 for burn wounds, and C1 and C2 for infected wounds. Excision wound models (A) received treatment from day one, while treatment for burn wound models (B) started from day 5 after burn skin removal. In infected wound models, treatment commenced from day two after

the onset of infection in the wounded area. The M4 thin film was applied to the wound surface using adhesive tape, and bandages were changed daily. Wound analysis was conducted, monitoring the progress of wound healing and closure at 2–3 day intervals until complete skin regeneration. Images of the wounds were captured throughout the study. The wound contraction percentage was calculated by using the following formula: where A_o is the area of the wound at day zero and A_n is the area of the wound at day 2, 4,6, etc.

$$\text{Wound Contraction } (\%) = [(A_o - A_n)/A_o] \times 100$$

Statistical analysis

Statistical analysis was carried out by using GraphPad Prism 9. All the data are stated as mean ± standard error of the mean (SEM) by using the row statistics program of GraphPad Prism.

Results and discussion

Thin films deposition

Five different formulations (M1, M2, M3, M4, M5) were prepared for thin film deposition by altering the combination of polymers, polymer concentrations, and the presence or absence of emulsifying agents as presented in Table 1. A schematic representation of the reactions and synthesis process for the thin film, including real images of the prepared samples, is provided in Fig. 1.

Initially, a solution of M1 was prepared by blending 1% CS, 1% CMC, and 0.5% TA in 50 mL of 1% acetic acid solution. After the evaporation of the solvent, a non-uniform thin film was obtained (Supplementary file S. Figure S1a). In M2, the same polymer formulation was used, but this time 0.2% glycerol and 0.2% Tween80 were added. By this time, a uniform thin film was synthesized on the glass surface but proved challenging to peel off (Fig. 2a). However, when immersed in water for 2 h, it transformed into a fabric-like membrane and was easily removed from the glass surface (Fig. 2b). In M3, the concentrations of polymers were doubled, i.e., 2% CS, 2% CMC, and 1% TA. Consequently, the film acquired a dark brown colour and was thick enough to be peeled off from the glass surface with a plastic-like appearance (Fig. 2c). The upper side of the film exhibited a rough surface, while the dorsal side that was in touch with the glass surface was smooth; however, the film lacked uniformity in appearance. In the subsequent attempt (M4), the same 2% CS, 2% CMC, and 1% TA were combined, but this time 0.2% glycerol and 0.2% Tween80 were added to achieve a homogeneous membrane. The solution was poured onto a glass plate (Supplementary file S. Figure S1b) and dried in an oven. A uniform brown-coloured thin film was obtained, which was easily peeled off from the glass surface (Fig. 2d,e). In the last attempt (M5), 1% BW was introduced in a combination of 1% CS, 1% CMC, 0.5% TA, to investigate the impact of beeswax on the gelling property of the film. During the drying process, a layer of BW was observed on the surface of the thin film, causing a delay in the evaporation process. The waxy appearance on the upper side of the film was attributed to the addition of beeswax (Fig. 2f).

As depicted in Fig. 2d,e, the formulation M4, consisting of 2% CS, 2% CMC, 1% TA, provided an excellent thin film with a uniform appearance aided by 0.2% glycerol acting as a plasticizer and 0.2% Tween80 serving as an emulsifying agent.

Characteristics of thin films

Thickness

Solid, brown to light brown coloured thin films (M1–5) with varying degrees of thickness and tensile strength were obtained as illustrated in (Fig. 2a–f). The films M2 and M5 exhibited nearly identical thicknesses of 23.10 ± 0.33 µm and 26.5 ± 0.22 µm, respectively. The thickness of M5 (26.5 ± 0.22 µm) was slightly greater due to the addition of 1% beeswax. The films M3 and M4, with double the concentration of ingredients, had thicknesses of 49.6 ± 0.68 µm and 39.0 ± 1.14 µm, respectively, which indicates that the film (M4) with a plasticizing agent (glycerol) and an emulsifying agent (tween80) has a reduced thickness compared to M3. However, by the addition of these agents, M4 achieved a more uniform, smoother and flexible structure as compared to M3. Furthermore, the thickness of the films increased upon water absorption, resulting in more flexible, soft, and sponge-like membranes with porous surfaces (Fig. 2b). The comparison of the thickness of films before and after swelling is depicted in a bar graph (Fig. 3a) and the data are given in Supplementary file S Table S1 and 2. The brownish colour of the film is attributed to the addition of tannic acid[21]. The thickness of the films increased with the rising concentration of ingredients. The thickness of the thin film obtained by the different researchers varies depending on the viscosity of the solution (due to the concentration of polymers) as well as the volume of solution spread on a specific area, for thin film deposition[28,35] Kaczmarek et al.. reported

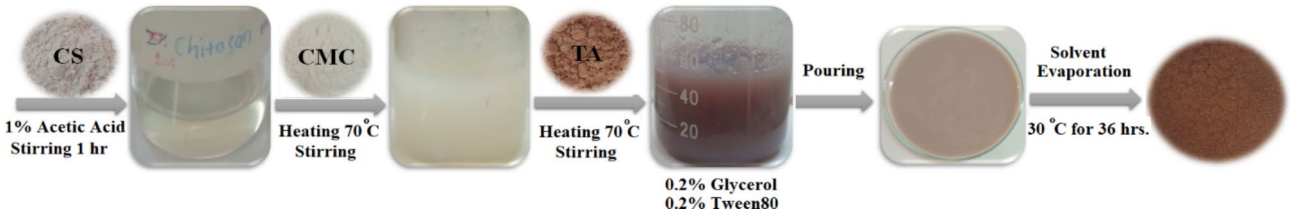

Fig. 1. Schematic diagram illustrating the synthesis process and reaction mechanisms involved in the preparation of the thin film.

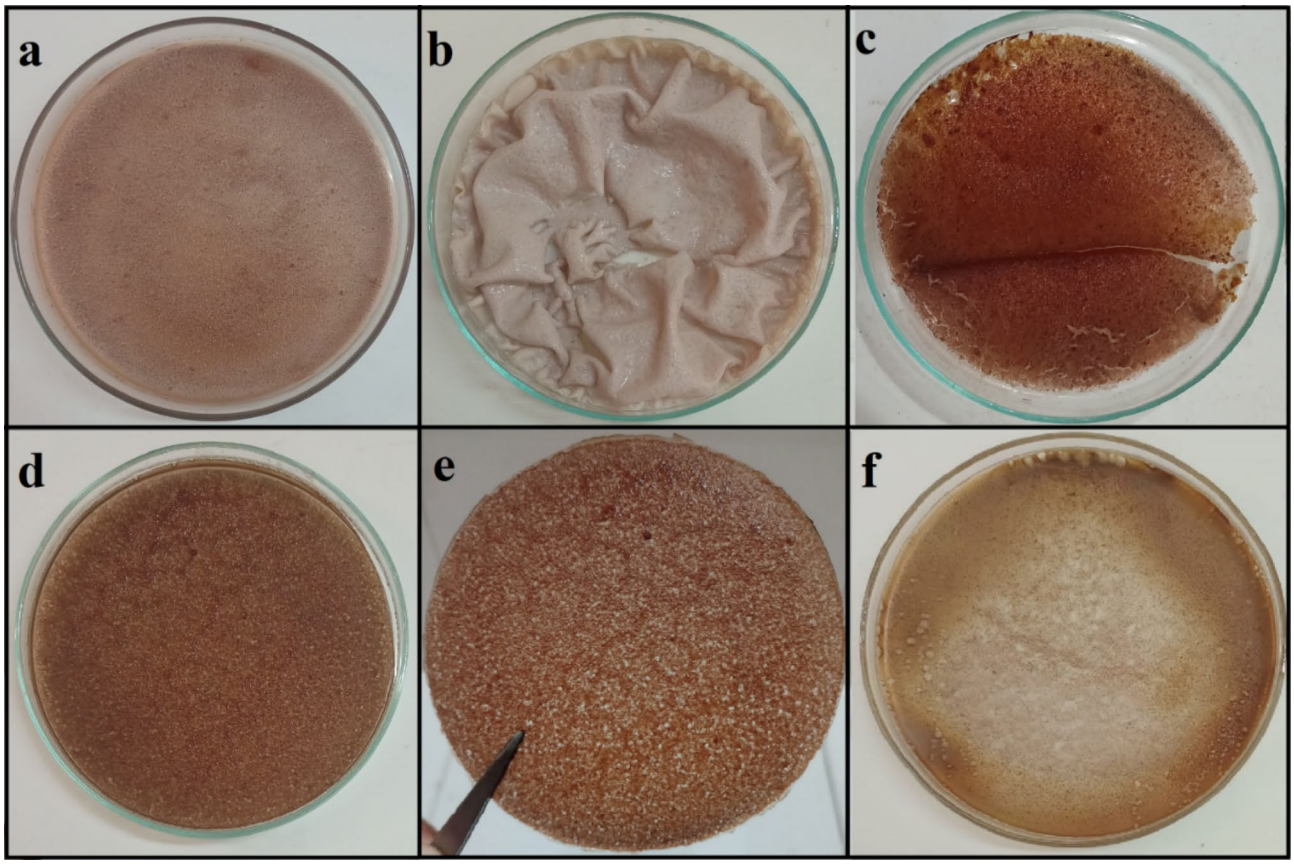

Fig. 2. (**a**) Deposition of thin film M2 on a glass surface, (**b**) M2 after wetting with water, (**c**) Non-uniform thin film deposition of M3, (**d**) Uniform deposition of M4 thin film, (**e**) M4 peeled-off from the glass plate, (**f**) M5 waxy thin layer with the addition of beeswax.

a chitosan/tannic acid thin film obtained by the same methodology of solvent evaporation deposition method with a thickness of 35 μm[19]. Sultan et al.. obtained a chitosan/beeswax/pollen grain composite thin film with a thickness of 38.9 ± 1.6 μm which closely aligns with our results[29].

Tensile strength

Thin films intended for wound healing applications should possess suitable mechanical properties and flexibility in both dry and wet states to facilitate optimal clinical operation and handling. The highest tensile strength, 0.275 ± 0.003 MPa, was observed in the M4 film. In contrast, M3 exhibited a tensile strength of 0.157 ± 0.003 MPa, M5 had a strength of 0.036 ± 0.004 MPa, and M2 showed a strength of 0.023 ± 0.002 MPa. The comparison of films according to their tensile strength is illustrated in the bar graph (Fig. 3b) and the data is provided in Supplementary File S. Table S3. The film M4 has a greater tensile strength (0.275 ± 0.003 MPa) compared to M3 due to the addition of glycerol and tween80. The maximum tensile strength of 3.93 MPa was achieved by Liang et al.. with chitosan-royal gel (5% RG)[8]. Adeli et al.. reported tensile strength of 1.33–6.15 MPa for nanofibrous mats of PVA/chitosan/starch[1]. Sultan et al. observed tensile strength of 0.77 MPa for the chitosan thin film[29]. Kaczmarek et al.. reported almost 3–22 MPa tensile strength of chitosan/tannic acid thin film based on their weight ratio[19].

Swelling degree

The swelling degree of each thin film was assessed after soaking in water for 2 h, the data is given in Supplementary File S. Table S4. The variation in swelling degree was observed based on the type of film. The film M4 demonstrated a higher percentage of swelling degree of 283.0 ± 2.0% within 2 h (Fig. 3c). In contrast, the film containing beeswax (M5) exhibited the minimum percentage swelling degree at 118.33 ± 1.67%. Results indicate that the films containing glycerol and tween80 (M2 and M4) has more porous structure due to which they absorb more water and high swelling capacity. Saragih et al.. reported a swelling degree of 137% with chitosan-cellulose nano-fiber hydrogel[25]. Sultan et al.. investigated a swelling degree of 458.8% with chitosan/beeswax/pollen grains thin film[36]. Xu et al. observed a water absorption capacity of greater than 400% for chitosan, tannic acid, and pullulan composite nanofibers' membranes[18].

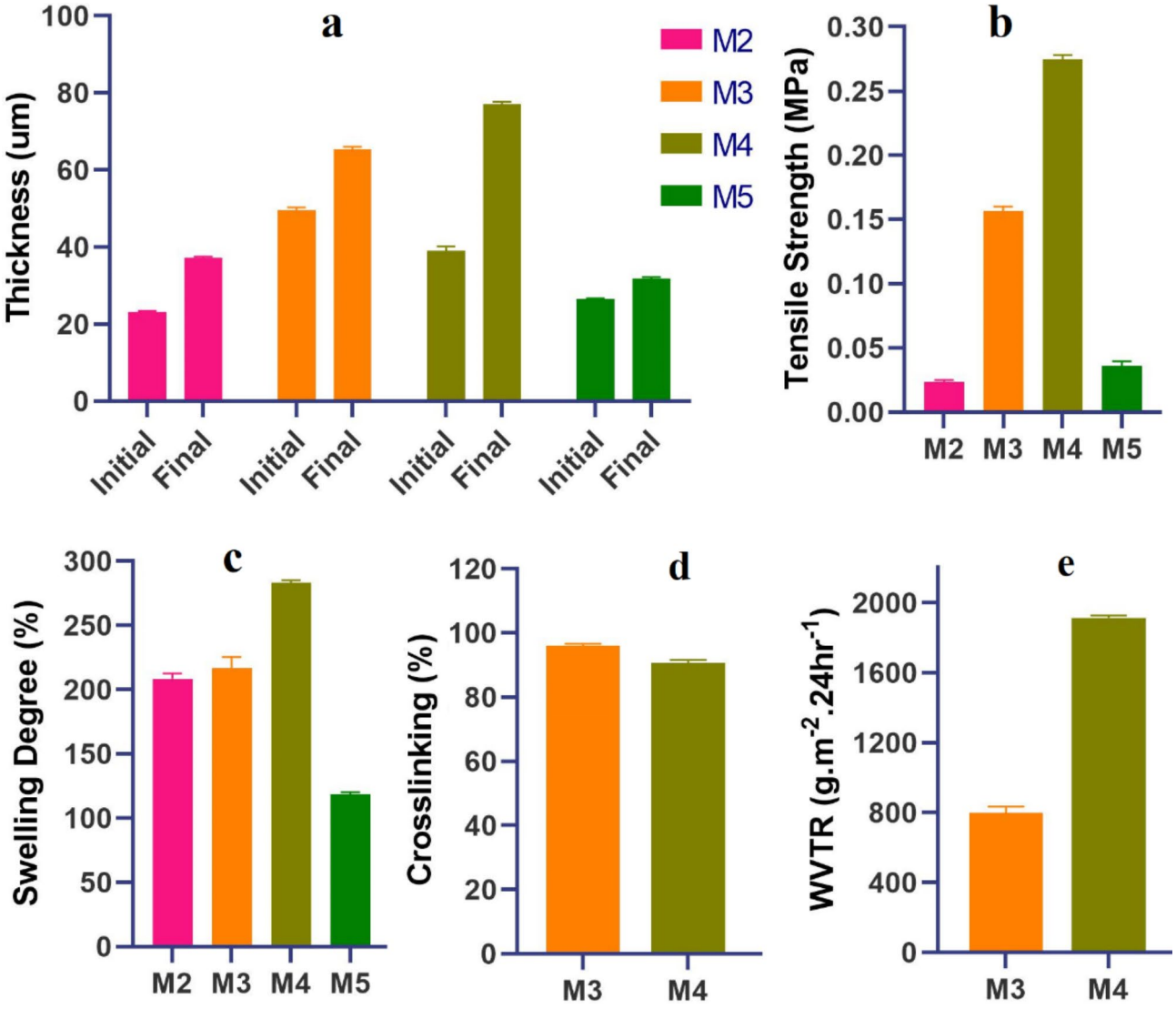

Fig. 3. (**a**) Comparison of thickness of thin films M2, M3, M4 and M5 before and after swelling, (**b**) Tensile strength of these thin films in (MPa), (**c**) Percentage swelling degree of thin films, (**d**) crosslinking percentage comparison of M3 and M4, (**e**) water vapor transmission rate of M3 and M4.

Contact angle

The contact angle represents the hydrophilic nature and surface energy of films. The lowest contact angle, possessing the highest surface energy was represented by M4 film with an average of 40.5°. The angle was almost similar on both, rough and smooth surfaces. The film, M3 represented a contact angle of 55°, M2 represented 59°, whereas M5 represented the highest contact angle of 86.5° (S. Figure 2a–d). Parin et al. reported a water contact angle of 48.3 ± 2.4° for a thin film of polyvinyl alcohol, inulin, and pumpkin powder (PIP) indicating its hydrophilic nature[32] The films with low contact angle represents a hydrophilic nature, good wettability, adhesiveness, and high solid surface energy and vice versa. The film, M4 represented the lowest contact angle due to its more jelling property and high surface energy by the addition of glycerol and tween 80. The smooth surface results from contact with the glass surface, while the rough surface is formed as a result of solvent evaporation from the upper surface.

Degree of crosslinking

To evaluate the degree of crosslinking in M3 and M4 thin films, the crosslinking percentage was determined as given in Supplementary File S. Table S5. It was observed that the crosslinking percentage of M4 (90.69 ± 0.83%) was slightly lower than that of M3 (96.06 ± 0.62%), as illustrated in the bar graph (Fig. 3d). The degree of crosslinking in M4 (90.69 ± 0.83%) was slightly lower than M3. Saragih et al.. observed a 90% degree of crosslinking in the chitosan-CNF hydrogel[25]. Our results suggest that the addition of glycerol and Tween80 reduces the degree of crosslinking among polymers. This finding aligns with several studies that have been reported previously[37].

Water vapor transmission rate

The WVTR plays a crucial role in moisture management. The WVTR of thin films comprising M3, M4, and M5 was determined, as illustrated in bar graph (Fig. 3e) and the data is tabulated in Supplementary File S. Table S6. Specifically, the WVTR of M4 was 1912.25 ± 13.10 g m^{-2} 24 h^{-1}, greater than that of M3 (798.95 ± 34.65) and M5 (1532.42 ± 22.69). It is noteworthy that the optimal WVTR range for an ideal wound healing environment falls between 2000 and 2500 (g m^{-2} 24 h^{-1}). Elevated WVTR values expedite the drying process, potentially leading to scar formation[1]. In our case, the WVTR of M4 (1912.25 ± 13.10 g m^{-2} 0.24 h^{-1}) closely aligns with the ideal range. Kaczmarek et al. reported maximum WVTR of 1367.28 g m^{-2} 0.24 h^{-1} with 50/50 chitosan/tannic acid thin film[18]. According to them, the addition of tannic acid improves porosity and WVTR[18]. Our results indicate that WVTR further increases by the addition CMC in CS/TA thin film due to increase in porosity. Sultan et al.. estimated the WVTR of 2065.23 g m^{-2} 0.24 h^{-1} with CS thin film, whereas 1038.07 g m^{-2} 0.24 h^{-1} with chitosan/beeswax/pollen grains composite thin film[36].

Drug release capacity

The sustained drug release is another important factor for the healing of wounds and infections. In this study, the release of TA in water was determined for M3 and M4 thin films by measuring absorption at 276 nm at various time intervals, data is given in Supplementary File, S. Table S7a,b. The percentage of drug release was calculated relative to the initial concentration of tannic acid in the thin film and the plot of the percentage of drug release over time is depicted (Fig. 4a). Initially, the rate of drug release was rapid for up to 2 h, followed by a gradual slowing down in the subsequent 2–4 h, reaching an almost constant level up to 24 h. The rate of drug release was higher in M4 compared to M3, attributed to its greater percentage porosity, hydrophilic nature, greater surface area, and enhanced swelling percentage in water. After 24 h, the drug release percentage of M3 was 53%, whereas in M4 it was 89.4%. According to Guarnizo-Herrero et al.. chitosan-carboxymethyl cellulose interpolymer complex matrix tablets are good drug carriers and drug release can be sustained for 8 h[12]. However, they observed a very fast drug release percentage of 90.64 ± 4.16% at 30 min for CL: (CS) 80:(20).

The drug release profile of the M4 thin film was further analyzed using the Higuchi Model (Diffusion-controlled release), which describes an initial rapid release of the drug followed by a slower release governed by diffusion through the matrix. The data was analyzed using linear regression in GraphPad Prism 9, with corresponding data provided in Supplementary File, S. Table S7c. The goodness of fit, R^2, was 0.9859 and the data was statistically significant with a p-value of < 0.0001 and an F value of 911.7. The graph representing the Higuchi kinetics is shown in Fig. 4b.

FT-IR analysis of thin film

FT-IR analysis of M4 thin film was conducted to examine the interaction between various polymers and their cross-linking. The spectrum of the M4 thin film was compared with the reference polymers, including CS, CMC, and TA (Fig. 5a). The M4 spectrum exhibited distinct absorption peaks and intensities compared to those of the reference polymers (CS, CMC, TA). The FT-IR spectra and absorption bands of CS, CMC, and TA are well-known and reported in the literature (Fig. 5b)[38,39,40] The variations in the M4 spectrum from the reference peaks are further illustrated in Fig. 5c. The absorption band at 3426 cm^{-1} in M4 seems to be shifted towards a higher absorption frequency compared to the reference polymers, which suggests N-H stretching due to amide linkage, which aligns with the formation of a cross-linked structure[41,42]. The sharp peaks at 2928 cm^{-1} and 2856 cm^{-1} are attributed to C–H stretching, with the later associated with the C–H stretch of the carbonyl group due to aldehyde/amide functional groups. These intense peaks also indicate the presence of dimers due to hydrogen bonding. The peak at 1705 cm^{-1} is attributed to the C=N stretching of the secondary amide group, while the

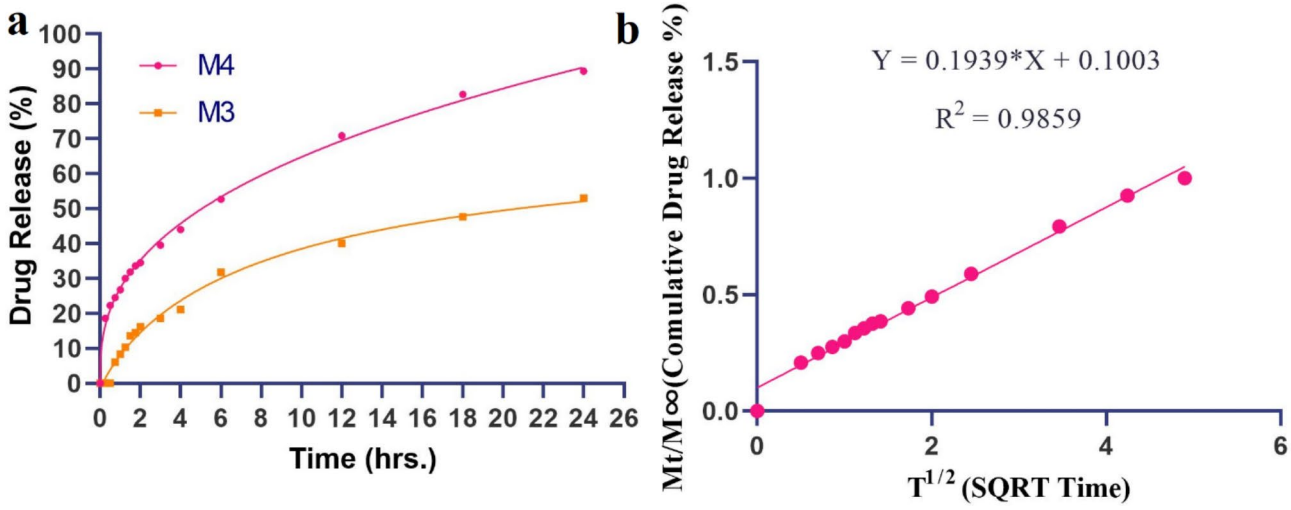

Fig. 4. (**a**) Drug release percentage of thin films M3 and M4. (**b**) Higuchi kinetic model for drug release (cumulative drug release percentage vs. square root (SQRT) of time).

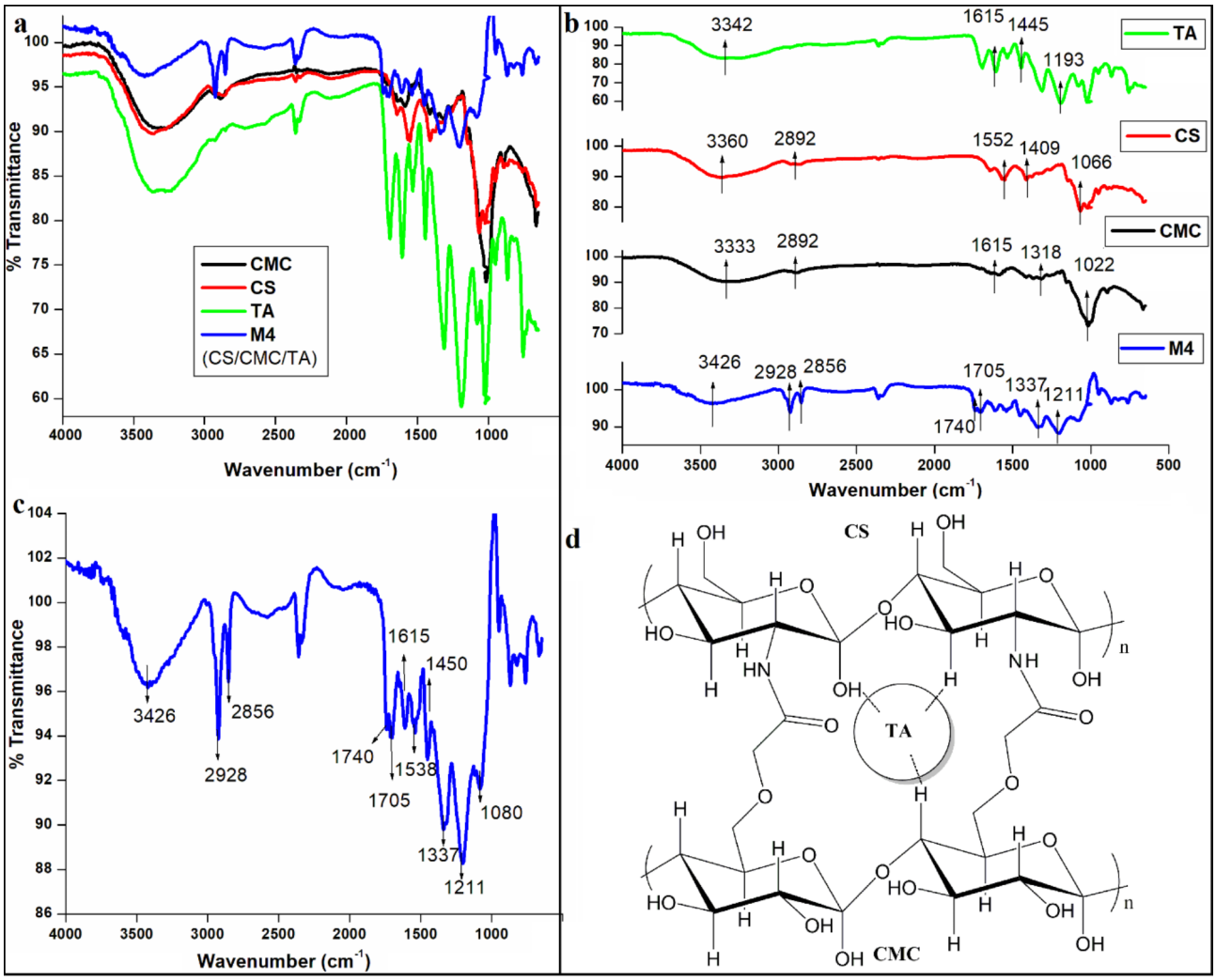

Fig. 5. (**a**) Comparison of FT-IR spectra of CS, CMC, TA and M4 thin film, (**b**) FT-IR Spectra in different layers and their major absorption bands, (**c**) FT-IR spectrum of M4 thin film with its absorption bands, (**d**) Proposed molecular level structure of M4 thin film with most probable crosslinking and interaction between different polymers (Black dotted lines represents hydrogen bonding between tannic acid and other polymers).

peak at 1740 cm^{-1} corresponds to the C=O stretching. Both new peaks are indicative of the secondary amide and potential contributions from acetic acid, which further confirms the chemical interactions taking place in the M4 formulation[41]. The strong absorption peak at 1211 cm^{-1} in the M4 thin film represents C–N stretching of the secondary amide[41]. The band at 1538 cm^{-1} is attributed to N–H bending vibrations of the secondary amide, and the peak at 1615 cm^{-1} is attributed to C=O stretching vibrations of the amide group[41]. The more pronounced peak at 1337 cm^{-1} is attributed to O–H bending vibrations, indicating the presence of a large amount of -OH functional groups in CS, CMC, and TA[38].

Based on these spectra, it can be inferred that CS and CMC are likely to be cross-linked via amide linkages, with tannic acid present in the spaces contributing to the hydrogen bonding network. All three are also interconnected through hydrogen bonding. The most probable molecular structure of the M4 thin film is illustrated in Fig. 5d. Several studies have reported the interaction of chitosan and carboxymethyl cellulose through XRD and FT-IR analysis. Guarnizo-Herrero et al.. observed the electrostatic attractions between the ionized amino (NH_3^+) group of chitosan and the carboxylic (COO^-) groups of the anionic carboxymethyl cellulose through SEM, FT-IR, and XRD[11]. Valizadeh et al.. synthesized bioactive composite film from chitosan and carboxymethyl cellulose using glutaraldehyde, cinnamon essential oil and oleic acid as crosslinkers[15]. Uyanga and Daoud investigated the crosslinking effect of fumaric acid, tartaric acid, citric acid and zinc ions on carboxymethyl cellulose-chitosan composite hydrogel[22].

Microstructure of thin films

A stereomicroscope was used to examine the exterior structures of thin films[32]. The microstructure was observed to evaluate the effect of incorporating glycerol and tween80, and beeswax. The surface of M3, M4 and M5 was examined under compound microscope at 5× magnification and it was observed that the M4 film was more

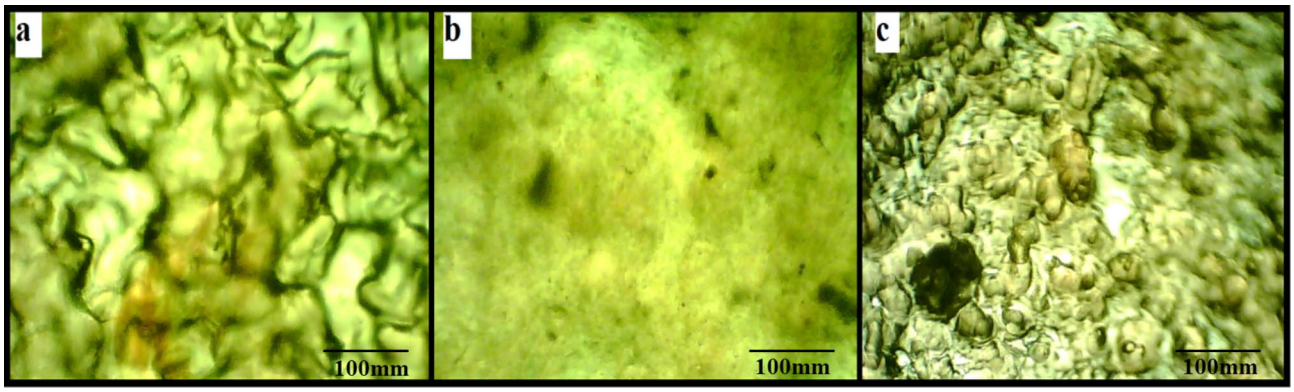

Fig. 6. Microstructures of thin films (**a**) M3, (**b**) M4 and (**c**) M5 at a magnification of ×5 obtained through a compound microscope.

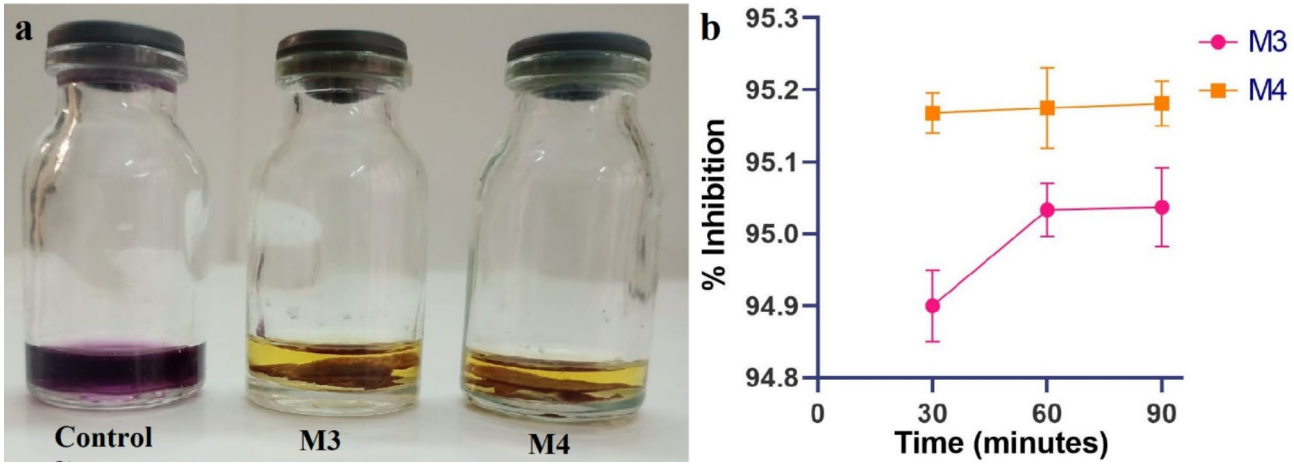

Fig. 7. DPPH free radical scavenging activity (**a**) comparison of inhibition of M3 and M4 with the control. (**b**) Effect on percentage inhibition at different time intervals.

smooth and uniform as compared to M3 and M5 (Fig. 6a–c). The surface compactness and uniformity was increased by adding the glycerol and tween80.

Antioxidant activity

To provide an insight into the release of antioxidant constituents, the DPPH free radical scavenging activity of M3 and M4 thin films was performed as a function of time. Both M3 and M4 exhibited outstanding antioxidant activity, with M4 demonstrating marginally higher activity than M3. Following a 30-min incubation, M3 displayed a percentage inhibition of $94.90 \pm 0.03\%$, while M4 exhibited a slightly higher inhibition of $95.17 \pm 0.02\%$. In the case of M4, the maximum inhibition was attained at 30 min and maintained at a consistent level. In contrast, in M3, the inhibition showed a slight increase up to 60 min and then became constant (Fig. 7a,b). The corresponding data is presented in Supplementary File S. Table S8. The antioxidant activity of CS and TA is well-known and reported in various studies[17,43]. According to Valizadeh et al. the antioxidant activity of CS-CMC film is due to the presence of the free NH_2 groups along the chitosan backbone which can react with free radicals and the protonation of $-NH_2$ to $-NH_3^+$ plays the main role in the antioxidant properties[16]. However, CMC has no antioxidant activity in itself. The incorporation of TA further enhances the antioxidant activity[19].

Antibacterial activity

The antibacterial efficacy of the M4 thin film was evaluated against Gram-positive bacteria (*S. aureus*) and Gram-negative bacteria (*E. coli*) using the disc diffusion method. Both of these strains are prevalent causes of skin and wound infections, disrupting the natural healing process. The M4 film exhibited significant inhibition against *S. aureus* and moderate inhibition against *E. coli* (Fig. 8a,b). A zone of inhibition measuring 19.85 ± 0.076 mm was observed against *S. aureus*, compared to the control, amoxicillin, which had an inhibition zone of 24.56 ± 0.08 mm, indicating an inhibition efficiency of approximately 81%. In contrast, M4 demonstrated lower efficiency against *E. coli*, with an inhibition zone of 14.50 ± 0.09 mm, compared to amoxicillin, which had an

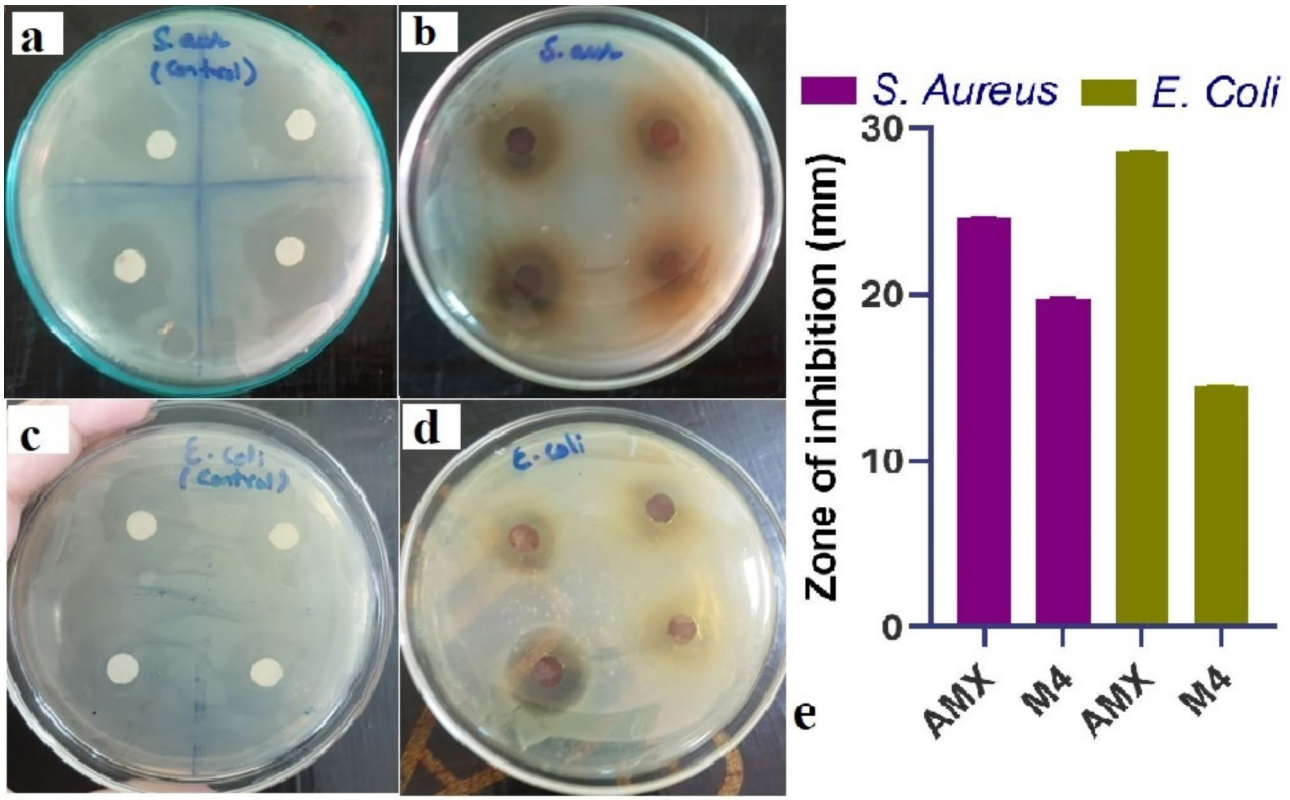

Fig. 8. (**a**) Zone of inhibition (mm) of M4 thin film against bacterial strains *S. aureus* and *E. coli* compared with control amoxicillin. (**b**) Bar-graph representing comparison of zone of inhibition of M4 against both strains.

inhibition zone of 28.62 ± 0.02 mm (Fig. 8c and d representing an efficiency of approximately 50%, as detailed in the Supplementary File, S. Table S9.

Similar findings were reported by Adeli et al.. using PVA/chitosan/starch nanofibrous mats, showing efficiency ranging from 60 to 84% against *S. aureus* and 47–72% against *E. coli*. These results suggest that thin films containing chitosan are more effective against Gram-positive bacteria than Gram-negative bacteria, likely due to differences in the cell wall structure of bacteria. The antibacterial properties of chitosan and tannins are well-documented in several reports[20,35,43].

Wound healing activity (In-vivo)

Wound healing activity was assessed using rabbit models A1 and A2 for excision wounds, B1 and B2 for burn wounds, and C1 and C2 for infected wounds, employing a thin film of M4 (S. Figure 3). For excision, burn, and infected wounds, scar formation occurred within 2–3 days after the start of treatment. Treatment continued until day 4, revealing the film's effectiveness in promoting scar formation and accelerating the healing process (Fig. 9). The film absorbed exudates from the burn and infected wounds, aiding in bacterial infection treatment and enhancing wound healing, leading to complete skin regeneration within 10–12 days (Fig. 9).

Wound closure for burn and infection was monitored at day 2, 4, 7, 10, and 12 until complete skin regeneration, as detailed in Supplementary File, S. Tables S10 and 11. The percentage of wound healing at day 7 was 90.0 ± 3.3% for burn wounds and 88.85 ± 1.7% for infected wounds, which increased further to 98.33 ± 1.7% and 99.35 ± 0.6% respectively, at day 10 (Fig. 10).

Significant progress in burn and infected wound recovery was observed from day one onwards. The film M4 stimulates blood vessel formation and epithelium formation. Treatment was discontinued at day 4, allowing for natural self-healing until complete skin regeneration occurred within 10–12 days. The percentage of wound healing at day 7 was 90.0 ± 3.3% for burn wounds and 88.85 ± 1.7% for infected wounds. Lu et al. observed wound healing activity of 57.46 ± 5.49% at day 9 in mice models by using gallic acid berberine self-assembled nanoparticles[33]. In assessing wound healing activity, we noted that the film demonstrates greater efficacy in moist and wet conditions. Specifically, its effectiveness is more pronounced during the first one to two days following the onset of a wound, especially when the wound is wet, infected, or emitting exudates and blood. Complete skin regeneration occurs within 10–12 days after the start of treatment in all cases, whether it is an excision, burn, or infected wound.

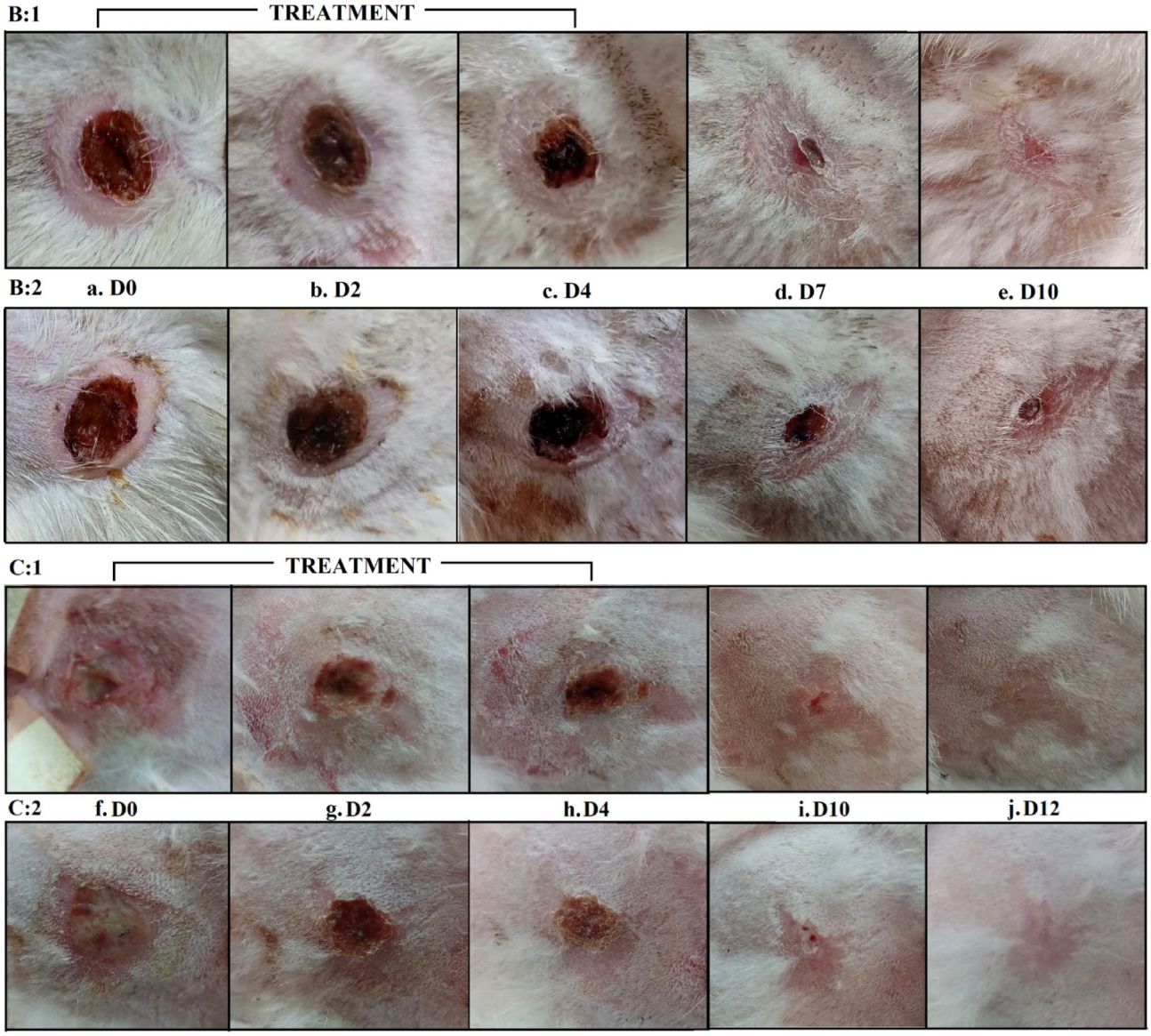

Fig. 9. Burn wound models (B1 and B2), their treatment and healing activity. (**a**) Burn wounds before treatment, (**b**) wound healing at day 2 and (**c**) wound healing and scar formation at day 4, (**d**,**e**) skin regeneration process. Infected wound models (C1 and C2), their treatment and healing process. (**f**) Infected wounds before treatment, (**g**) wound healing at day 2 and (**h**) wound healing and scar formation at day 4, (**i**,**j**) skin regeneration process.

Conclusion

In conclusion, the formulated M4 thin film, composed of chitosan, carboxymethyl cellulose, and tannic acid, demonstrated exceptional mechanical strength, high swelling capacity, efficient drug release, and strong bioactivity, including antioxidant and antibacterial properties. The FT-IR analysis confirmed cross-linking through amide linkages and hydrogen bonding, contributing to the film's structural stability. The in-vivo rabbit model showed rapid wound healing for both burn and infected wounds, with over 90% recovery by day 7 and complete skin regeneration within 10–12 days. These findings highlight the film's potential as an effective wound dressing that protects against pathogens while promoting faster tissue repair. The promising results pave the way for further exploration of this formulation in treating infections and developing innovative therapeutic solutions for wound care. In light of these findings, our upcoming research will focus on investigating the efficacy of the M4 formulation in the treatment of cancer.

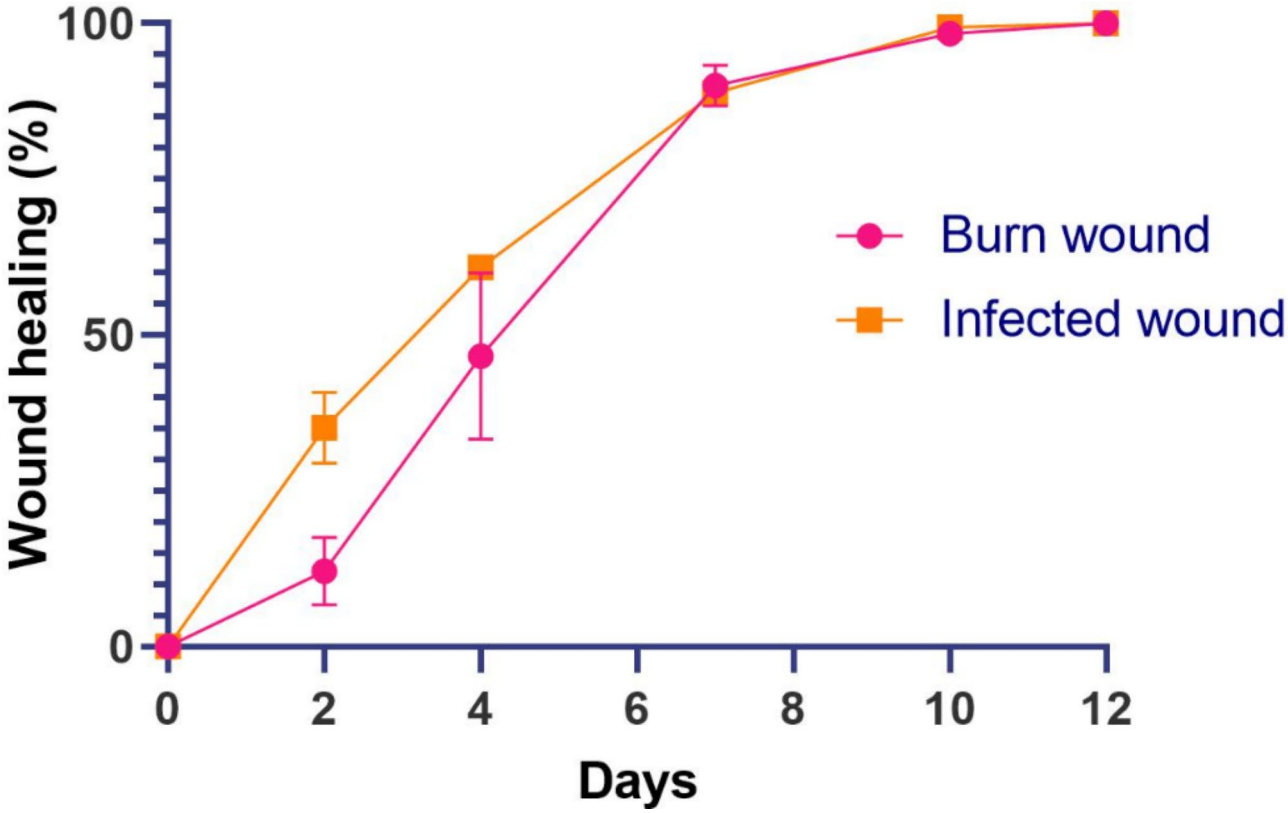

Fig. 10. Percentage healing of burn wound and infected wound in a number of days.

Data availability

All the data are included within the manuscript and supplementary file. Raw data can be obtained from the corresponding author upon reasonable request.

Received: 2 August 2024; Accepted: 6 November 2024
Published online: 09 November 2024

References

1. Adeli, H., Khorasani, M. T. & Parvazinia, M. Wound dressing based on Electrospun PVA/Chitosan/Starch Nanofibrous mats: fabrication, antibacterial and cytocompatibility evaluation and in Vitro Healing Assay. *Int. J. Biol. Macromol.* **122**, 238–254. https://doi.org/10.1016/j.ijbiomac.2018.10.115 (2019).
2. Boateng, J. & Catanzano, O. Advanced therapeutic dressings for effective wound healing—a review. *J. Pharm. Sci.* **104** (11), 3653–3680. https://doi.org/10.1002/jps.24610 (2015).
3. Khorasani, M. T., Joorabloo, A., Moghaddam, A., Shamsi, H. & MansooriMoghadam, Z. Incorporation of ZnO nanoparticles into heparinised polyvinyl alcohol/chitosan hydrogels for wound dressing application. *Int. J. Biol. Macromol.* **114**, 1203–1215. https://doi.org/10.1016/j.ijbiomac.2018.04.010 (2018).
4. Alven, S. & Aderibigbe, B. A. Chitosan and cellulose-based hydrogels for wound management. *Int. J. Mol. Sci.* **21** (24), 9656. https://doi.org/10.3390/ijms21249656 (2020).
5. Baghaie, S., Khorasani, M. T., Zarrabi, A. & Moshtaghian, J. Wound healing properties of PVA/Starch/Chitosan hydrogel membranes with nano zinc oxide as antibacterial wound dressing material. *J. Biomater. Sci. Polym. Ed.* **28** (18), 2220–2241. https://doi.org/10.1080/09205063.2017.1390383 (2017).
6. Oryan, A. & Sahvieh, S. Effectiveness of chitosan scaffold in skin, bone and cartilage healing. *Int. J. Biol. Macromol.* **104**, 1003–1011. https://doi.org/10.1016/j.ijbiomac.2017.06.124 (2017).
7. Bandyopadhyay, S., Saha, N., Brodnjak, U. V. & Sáha, P. Bacterial cellulose and guar gum based modified PVP-CMC hydrogel films: characterized for packaging fresh berries. *Food Packag. Shelf Life*. **22**, 100402. https://doi.org/10.1016/j.fpsl.2019.100402 (2019).
8. Liang, H., He, X., Li, X., Semiruomi, D. & Yan, F. Effect of royal gel addition to chitosan matrix for wound dress applications: fabrication, characterization and artificial neural network analysis. *Environ. Technol. Innov.* **30**, 103077. https://doi.org/10.1016/j.eti.2023.103077 (2023).
9. Hasegawa, M., Isogai, A., Onabe, F., Usuda, M. & Atalla, R. H. Characterization of cellulose–chitosan blend films. *J. Appl. Polym. Sci.* **45** (11), 1873–1879. https://doi.org/10.1002/app.1992.070451101 (1992).
10. Abu Elella, M. H. & Kolawole, O. M. Recent advances in modified chitosan-based drug delivery systems for transmucosal applications: a comprehensive review. *Int. J. Biol. Macromol.* **277**, 134531. https://doi.org/10.1016/j.ijbiomac.2024.134531 (2024).
11. Asanarong, O., Minh Quan, V., Boonrungsiman, S. & Sukyai, P. Bioactive wound dressing using bacterial cellulose loaded with papain Composite: morphology, loading/release and antibacterial properties. *Eur. Polym. J.* **143**, 110224. https://doi.org/10.1016/j.eurpolymj.2020.110224 (2021).
12. Guarnizo-Herrero, V. et al. Study of different chitosan/sodium carboxymethyl cellulose proportions in the development of polyelectrolyte complexes for the sustained release of clarithromycin from matrix tablets. *Polymers*. **13** (16), 2813. https://doi.org/10.3390/polym13162813 (2021).

13. Aravamudhan, A., Ramos, D. M., Nada, A. A. & Kumbar, S. G. Natural polymers. In *Natural and Synthetic Biomedical Polymers* 67–89. https://doi.org/10.1016/B978-0-12-396983-5.00004-1 (Elsevier, 2014).
14. Abdel-Raouf, M. E. S. et al. Chitosan-based architectures as an effective approach for the removal of some toxic species from aqueous media. *ACS Omega*. **8** (11), 10086–10099. https://doi.org/10.1021/acsomega.2c07264 (2023).
15. Rachtanapun, P. et al. Effect of monochloroacetic acid on properties of carboxymethyl bacterial cellulose powder and film from nata de coco. *Polymers*. **13** (4), 488. https://doi.org/10.3390/polym13040488 (2021).
16. Valizadeh, S., Naseri, M., Babaei, S., Hosseini, S. M. H. & Imani, A. Development of bioactive composite films from chitosan and carboxymethyl cellulose using glutaraldehyde, cinnamon essential oil and oleic acid. *Int. J. Biol. Macromol.* **134**, 604–612. https://doi.org/10.1016/j.ijbiomac.2019.05.071 (2019).
17. Fraga-Corral, M. et al. Technological application of tannin-based extracts. *Molecules*. **25** (3), 614. https://doi.org/10.3390/molecules25030614 (2020).
18. Xu, F., Weng, B., Gilkerson, R., Materon, L. A. & Lozano, K. Development of tannic acid/chitosan/pullulan composite nanofibers from aqueous solution for potential applications as wound dressing. *Carbohydr. Polym.* **115**, 16–24. https://doi.org/10.1016/j.carbpol.2014.08.081 (2015).
19. Kaczmarek, B., Nadolna, K., Owczarek, A., Michalska-Sionkowska, M. & Sionkowska, A. The characterization of thin films based on chitosan and tannic acid mixture for potential applications as wound dressings. *Polym. Test.* **78**, 106007. https://doi.org/10.1016/j.polymertesting.2019.106007 (2019).
20. Scalbert, A. Antimicrobial properties of tannins. *Phytochemistry*. **30** (12), 3875–3883. https://doi.org/10.1016/0031-9422(91)83426-L (1991).
21. Yang, D. et al. Hydrogel wound dressings containing bioactive compounds originated from traditional Chinese herbs: a review. *Smart Mater. Med.* **5** (1), 153–165. https://doi.org/10.1016/j.smaim.2023.10.004 (2024).
22. Uyanga, K. A., Daoud, W. A., Green and sustainable carboxymethyl cellulose-chitosan composite hydrogels. Effect of crosslinker on microstructure. *Cellulose*. **28** (9), 5493–5512. https://doi.org/10.1007/s10570-021-03870-2 (2021).
23. Nur Parin, F. & Deveci, S. Production and characterization of bio-based sponges reinforced with *Hypericum Perforatum* Oil (St. John′s Wort Oil) via pickering emulsions for wound healing applications. *ChemistrySelect* **8**(5), e202203692. https://doi.org/10.1002/slct.202203692 (2023).
24. Abdallah, H. M., Abu Elella, M. H. & Abdel-Aziz, M. M. One-pot green synthesis of chitosan biguanidine nanoparticles for targeting *M. tuberculosis*. *Int. J. Biol. Macromol.* **232**, 123394. https://doi.org/10.1016/j.ijbiomac.2023.123394 (2023).
25. Ali, M., Shakeel, M. & Mehmood, K. Extraction and characterization of high purity chitosan by rapid and simple techniques from mud crabs taken from Abbottabad. *Pak. J. Pharm. Sci.* (2019).
26. Foo, S. Y., Nur Hanani, Z. A., Rozzamri, A., Ibadullah, W. Z. W. & Ismail-Fitry, M. R. Effect of chitosan–beeswax edible coatings on the shelf-life of Sapodilla (Achras Zapota) Fruit. *J. Packag. Technol. Res.* **3** (1), 27–34. https://doi.org/10.1007/s41783-018-0047-0 (2019).
27. Velickova, E., Winkelhausen, E., Kuzmanova, S., Alves, V. D. & Moldão-Martins, M. Impact of chitosan-beeswax edible coatings on the quality of fresh strawberries (Fragaria Ananassa Cv Camarosa) under commercial storage conditions. *LWT Food Sci. Technol.* **52** (2), 80–92. https://doi.org/10.1016/j.lwt.2013.02.004 (2013).
28. Saragih, S. W., Wirjosentono, B. & Eddiyanto; Meliana, Y. Influence of crosslinking agent on the morphology, chemical, crystallinity and thermal properties of cellulose nanofiber using steam explosion. *Case Stud. Therm. Eng.* **22**, 100740. https://doi.org/10.1016/j.csite.2020.100740 (2020).
29. Merchant, H. A., Shoaib, H. M., Tazeen, J. & Yousuf, R. I. Once-daily tablet formulation and in vitro release evaluation of cefpodoxime using hydroxypropyl methylcellulose: a technical note. *AAPS PharmSciTech*. **7** (3), E178–E183. https://doi.org/10.1208/pt070378 (2006).
30. Ekenna, I. C. & Abali, S. O. Comparison of the use of kinetic model plots and DD solver software to evaluate the drug release from griseofulvin tablets. *J. Drug Deliv. Ther.* **12** (2-S), 5–13. https://doi.org/10.22270/jddt.v12i2-S.5402 (2022).
31. Baskar, R., Shrisakthi, S., Sathyapriya, B., Shyampriya, R., Nithya, R.,Poongodi, P. Antioxidant potential of peel extracts of banana varieties(*Musa Sapientum*). *Food Nutr. Sci.* **02** (10), 1128–1133. https://doi.org/10.4236/fns.2011.210151 (2011).
32. Parın, F. N. et al. PVA/Inulin-based sustainable films reinforced with pickering emulsion of niaouli essential oil for potential wound healing applications. *Polymers*. **15** (4), 1002. https://doi.org/10.3390/polym15041002 (2023).
33. Parın, F. N. et al. Development of PVA–Psyllium husk meshes via emulsion electrospinning: preparation, characterization, and antibacterial activity. *Polymers*. **14** (7), 1490. https://doi.org/10.3390/polym14071490 (2022).
34. Wang, P., Yan, S. T., Xu, H. G., Xu, X. L. & Zheng, W. J. Anion photoelectron spectroscopy and density functional theory studies of AuC n –/0 (n = 3 – 8): odd-even alternation in Electron binding energies and structures. *Chin. J. Chem. Phys.* **35** (1), 177–184. https://doi.org/10.1063/1674-0068/cjcp2112267 (2022).
35. Strnad, S. & Zemljič, L. Cellulose–chitosan functional biocomposites. *Polymers* **15**(2), 425. (2023). https://doi.org/10.3390/polym15020425
36. Sultan, M., Hafez, O. M., Saleh, M. A. & Youssef, A. M. Smart edible coating films based on chitosan and beeswax–pollen grains for the postharvest preservation of Le Conte Pear. *RSC Adv.* **11** (16), 9572–9585. https://doi.org/10.1039/D0RA10671B (2021).
37. Chavda, H. & Patel, C. Effect of crosslinker concentration on characteristics of superporous hydrogel. *Int. J. Pharm. Investig.* **1** (1), 17. https://doi.org/10.4103/2230-973X.76724 (2011).
38. Drabczyk, A. et al. Physicochemical investigations of Chitosan-based hydrogels containing Aloe Vera designed for biomedical use. *Materials*. **13** (14), 3073. https://doi.org/10.3390/ma13143073 (2020).
39. Mondal, M. I. H., Yeasmin, M. S. & Rahman, M. S. Preparation of food grade carboxymethyl cellulose from Corn Husk Agrowaste. *Int. J. Biol. Macromol.* **79**, 144–150. https://doi.org/10.1016/j.ijbiomac.2015.04.061 (2015).
40. Tangarfa, M., Semlali Aouragh Hassani, N. & Alaoui, A. Behavior and mechanism of tannic acid adsorption on the Calcite Surface: Isothermal, kinetic, and thermodynamic studies. *ACS Omega*. **4** (22), 19647–19654. https://doi.org/10.1021/acsomega.9b02259 (2019).
41. Ji, Y. et al. DFT-calculated IR spectrum amide I, II, and III band contributions of *N* -methylacetamide fine components. *ACS Omega*. **5** (15), 8572–8578. https://doi.org/10.1021/acsomega.9b04421 (2020).
42. Parker, F. S. Amides and amines. In *Applications of Infrared Spectroscopy in Biochemistry, Biology, and Medicine* 165–172. https://doi.org/10.1007/978-1-4684-1872-9_8. (Springer US, 1971).
43. Feng, T., Du, Y., Li, J., Hu, Y. & Kennedy, J. F. Enhancement of antioxidant activity of Chitosan by Irradiation. *Carbohydr. Polym.* **73** (1), 126–132. https://doi.org/10.1016/j.carbpol.2007.11.003 (2008).
44. Lu, J. et al. Carrier-free binary self-assembled nanomedicines originated from traditional herb medicine with multifunction to accelerate MRSA-infected wound healing by antibacterial, anti-inflammation and promoting angiogenesis. *Int. J. Nanomed.* **18**, 4885–4906. https://doi.org/10.2147/IJN.S422944 (2023).

Acknowledgements

The research was conducted at the Department of Chemistry, Government Postgraduate College No. 1, Abbottabad, under the auspices of the Department of Higher Education, Government of KPK, Pakistan. The authors extend their appreciation to the Researchers Supporting project number (RSPD2024R729), King Saud University, Riyadh Saudi Arabia for funding this project.

Author contributions

Conceptualization, methodology and experimentation done by M.A. M.A., S.U. and S.J. data curation and writing—original draft preparation done by K.H. M.S. and M.K.K.; writing—review and editing done by M.D., M.S., S.R., F.M.H., T.A. and H.A.; visualization, supervision and funding acquisition done by S.J., T.A. and S.R. All authors have read and agreed to the published version of the manuscript.

Funding

The authors extend their appreciation to the Researchers Supporting project number (RSP2024R729), King Saud University, Riyadh Saudi Arabia for funding this project. The funding body has no role in study design.

Declarations

Ethics approval and consent to participate

Approval for the research was obtained from the Institutional Animal Care and Use Committee (IACUC) with D. No. 116.

Competing interests

The authors declare no competing interests.

Additional information

Supplementary Information The online version contains supplementary material available at https://doi.org/10.1038/s41598-024-79121-8.

Correspondence and requests for materials should be addressed to M.A. or S.R.

Reprints and permissions information is available at www.nature.com/reprints.

Publisher's note Springer Nature remains neutral with regard to jurisdictional claims in published maps and institutional affiliations.